

A 200-Mbps 0.02-nJ/b Dual-Mode Inductive Coupling Transceiver for cm-Range Multimedia Application

Seulki Lee, *Student Member, IEEE*, Jerald Yoo, *Student Member, IEEE*, and Hoi-Jun Yoo, *Fellow, IEEE*

Abstract—A 200-Mbps 0.02-nJ/b dual-mode inductive coupling transceiver is proposed for cm-range multimedia application. The inductive link geometry and the advantage of the pulse-based inductive coupling are explained. In this paper, the parallel capacitor connected with the TX inductor, the intersymbol interference (ISI) reduction scheme, and the pulse generation scheme are newly proposed. The parallel capacitor connected with the TX inductor increases the transmitter impedance so that it enhances the transmission distance by twofold, and the ISI reduction scheme pushes data rate up to 200 Mbps. Moreover, the pulse generation scheme reduces the energy consumption as low as 0.02 nJ/b. Maximum data rate and energy consumption are achieved in simulation. The transceiver occupies 0.012 mm² in 0.25- μ m CMOS process.

Index Terms—Inductive coupling, low-power transceivers, near-field communication, short-range wireless communication.

I. INTRODUCTION

RECENTLY, wireless communications with short range (< 5 cm) and high data rate (> 100 Mbps) such as wireless personal area networks (WPANs) are widely used for battery-powered devices [1], [2]. Also, there is ongoing research about short-range wireless access for mutual communication between wireless devices [3], [4]. Since these applications are powered by battery, low-power consumption is one of the most important design issues. Although several existing wireless standards such as ZigBee, Bluetooth, and RFID are considered candidate solutions to these applications, they have fatal problems of low data rate and large power consumption. Fig. 1 shows the communication distance and the data rate of current wireless standards. Existing wireless communications show that their maximum data rate is only a few hundred kbps, which is too low for high-speed multimedia WPAN applications. Also, they consume power of a few hundred milliwatts [5], [6], which is unsuitable for multimedia WPANs. Ultra-wideband (UWB) shows the highest data rate up to a few hundred Mbps [5]. Especially in high-data-rate applications such as Internet access, multimedia services, or wireless peripheral interfaces and wireless body area network (WBAN) applications, UWB is regarded as a promising solution [2], even though it consumes

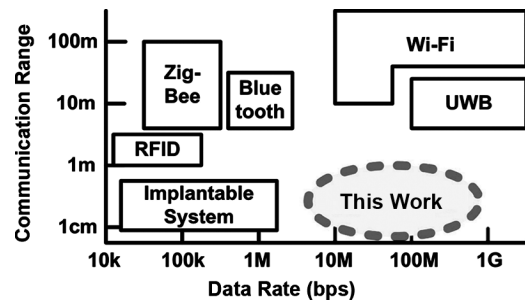


Fig. 1. Communication distance versus data rate of wireless standards.

high power. Currently, continuous research is underway on decreasing its power consumption [7]–[9]. However, UWB transceivers still consume as much as 236 mW [7], which is not acceptable for battery-powered devices such as portable multimedia WPAN applications. Although the impulse radio UWB (IR-UWB) transceiver does not consume a great deal of power [9], its communication distance is limited to only a few tens of micrometers, so that it is inappropriate for portable applications.

The conventional approaches consume much power due to their communication distance (> 1 m), as shown in Fig. 1. There are WPAN applications with only a few centimeters of communication range such as wearable computer systems or board-to-board communication systems [3], [4], [22], [28]. Inductive coupling transceivers are mostly used for the chip-to-chip communication system [10]–[13], and the implantable system [14]–[20] for only limited communication distance or limited data rate. Also, several inductive coupling transceivers were proposed [21]–[23], but none of them provide both high data rate and low-power consumption. Thus, a new low-energy cm-range transceiver with both low power and high data rate above 100 Mbps is needed for multimedia WPAN applications.

In this paper, we propose a dual-mode low-energy inductive coupling transceiver for high-speed multimedia applications. An effective intersymbol interference (ISI) reduction scheme can improve the data rate as much as 200 Mbps, and the energy consumption is only 0.02 nJ/b by the proposed pulse generation scheme. By employing an adaptively enabled parallel capacitor, the dual-mode transceiver can achieve low energy and extended communication range.

The remainder of this paper is organized as follows. In Section II, the inductive link with the pulse-based inductive coupling will be covered. Section III describes the operation of

Manuscript received September 29, 2008; revised December 29, 2008. First published February 13, 2009; current version published May 20, 2009. This paper was presented in part at the IEEE International Symposium on Circuits and Systems, Seattle, WA, May 18–21, 2008. This paper was recommended by Guest Editor A. Chan Carusone.

The authors are with the Department of Electrical Engineering and Computer Science, Korea Advanced Institute of Science and Technology (KAIST), Daejeon, 305-701, Korea (e-mail: sklee@eeinfo.kaist.ac.kr).

Digital Object Identifier 10.1109/TCSI.2009.2015209

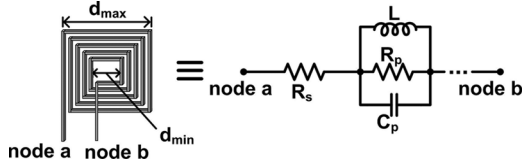


Fig. 2. *RLC* model of planar inductor.

the proposed transceiver, Section IV explains the design of the transceiver circuits, and Section V presents the performance evaluation. Finally, conclusions will be made in Section VI.

II. INDUCTIVE LINK

A. Inductor Geometry Consideration

Inductive coupling applications usually employ planar spiral type inductors made of monolithic metal wires, placed on chip for chip-to-chip communication systems [10], [11]. The board-to-board coupling inductors are drawn on printed circuit board (PCB) using thin metal patterns [12], [13]. The shapes of these inductors significantly limit the characteristics of the inductor such as inductance and size. To increase the inductance value or the communication range, pancake-type planar inductors are employed for this design [18]. Although the pancake-type inductor is not an exact planar inductor, it can be approximated as a planar inductor. Fig. 2 shows the shape of the typical planar inductor and its equivalent *RLC* model, with the outer diameter (d_{\max}) and the inner diameter (d_{\min}) of an inductor. For a pancake-type inductor, the following relationship exists between the magnitude of d_{\max} , d_{\min} , and the height of wire (h):

$$d_{\max} \cong d_{\min} \gg h. \quad (1)$$

The inductors of this design are made by copper wires coated with nonconductive material. Since $h \approx 100 \mu\text{m}$ and $d_{\min} > 1 \text{ mm}$, the inductor can be assumed as a planar inductor. The inductance of the planar spiral inductor is expressed as [24]

$$L = \frac{r^2 \cdot n^2}{8 \cdot r + 11 \cdot w_{\text{total}}} \quad (2)$$

where r represents the average radius ($(d_{\max} + d_{\min})/4$), w_{total} represents the total wire width of the inductor ($(d_{\max} + d_{\min})/4$), and n represents the number of turns. Equation (2) can be applied for the inductor with $w_{\text{total}} > 0.2r$. The fill ratio ρ represents how hollow the inductor is and is defined as

$$\rho = \frac{w_{\text{total}}}{r} \quad (3)$$

with small ρ for a hollow inductor ($d_{\max} \approx d_{\min}$) and large ρ for a full inductor ($d_{\max} \gg d_{\min}$). This parameter shows that two inductors with the same average diameter but different fill ratios will have different inductance values; a pancake-type inductor has larger inductance value than a spiral inductor type has.

As shown in Fig. 2, the *RLC* model of the inductor can be represented by the self-inductance L is expressed in (2), the

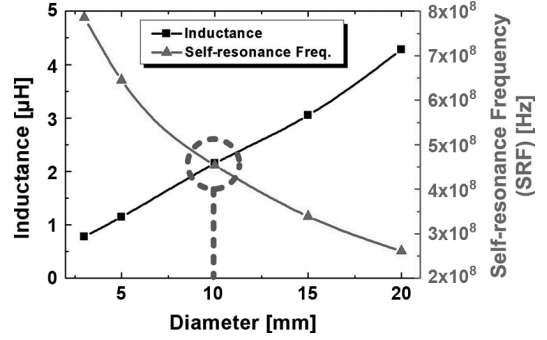


Fig. 3. Inductance and self-resonance frequency versus size of inductor (measured).

wire resistance R_S , and the parasitic components of the inductor C_P and R_P . R_P and C_P are related to self-resonance frequency (f_{SR}) and Q factor of an inductor. Although the model is very simple, it is fitted perfectly for the frequency band below f_{SR} , which is the region of concern in this study. The impedance between node a and node b is derived as follows:

$$\begin{aligned} Z_{ab} &= \left(j\omega L \parallel R_P \parallel \frac{1}{j\omega C} \right) + R_S \\ &= \frac{j\omega L(R_S + R_P) + R_S R_P(1 - \omega^2 L C_P)}{R_P(1 - \omega^2 L C_P) + j\omega L}. \end{aligned} \quad (4)$$

Its f_{SR} is derived as

$$f_{SR} = \frac{1}{2\pi\sqrt{L C_P}}. \quad (5)$$

Fig. 3 shows the relationship between the inductance value, the f_{SR} , and the inductor size. Considering the sizes of inductors that are used in [10]–[23], pancake-type square inductors with various sizes are designed to obtain more than $1\text{-}\mu\text{H}$ inductance, which is enough for the cm-range inductive coupling. As shown in Fig. 3, with the increasing inductor size, the inductance value increases but the f_{SR} decreases. Larger inductance, i.e., bigger inductor, makes the communication distance longer, and higher f_{SR} , i.e., smaller inductor, makes the data rate higher [13]. Since the tradeoff between the f_{SR} and the inductance also means the tradeoff between the data rate and the communication distance, they are very important parameters in this design.

The amplitude of the received voltage depends on the coupling coefficient k of the inductive link. By defining k as the ratio between input signal magnitude and the output signal magnitude, the received signal $V_{\text{out}}(t)$ is expressed by the transmitted signal $V_{\text{in}}(t)$ as

$$V_{\text{out}}(t) = k \cdot V_{\text{in}}(t). \quad (6)$$

Based on (6), the practical coupling coefficient k versus the communication distance between the transmitter and the receiver is measured as shown in Fig. 4. The measurements are performed for the various inductor diameters. From the measurement results, the following two propensities are found.

- 1) The coupling coefficient k is inversely proportional to the distance between inductors.

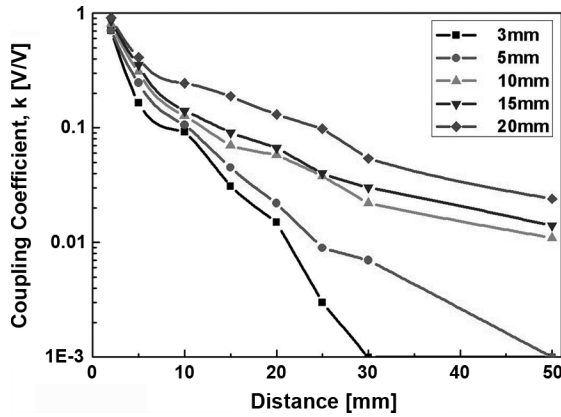


Fig. 4. Coupling coefficient k versus communication distance for the variety of inductor size (measured).

2) The amplitude of the received voltage is proportional to the diameter of the inductor size.

Inductor size affects the value of the coupling coefficient k according to the communication distance. For example, when $2.5 V_{p-p}$ input signal is applied, the received voltage magnitude of the 3-mm- and 5-mm-diameter inductors at 50-mm distance is measured as less than 0.001 V. However, the received voltage amplitude of the 10-, 15-, and 20-mm-diameter inductors at same communication distance is a few tens of millivolts. For this design, a 10-mm-diameter inductor is selected for both the transmitter and the receiver. The inductance is about $2 \mu H$ and the f_{SR} is around 400 MHz. Also, the coupling coefficient k is 0.0212 and 0.017 at distances of 30 and 59 mm, respectively. To achieve the communication range of up to several centimeters, the receiver must recover the signals as small as a few tens of millivolt levels with $2.5 V_{p-p}$ input signal.

B. Pulse-Based Inductive Coupling

There are two types of signals which are used in the communication through inductive link. One is the wideband signal without any carrier signal [10]–[13], and the other is narrowband signals with carrier signal [14]–[17]. For the communications that do not use proximity coupling, the narrowband signals with several modulation techniques such as ASK, OOK, FSK, or PSK are commonly used rather than wideband signals [25], [26]. The narrowband signal uses a carrier signal of a certain frequency such as 13.56 MHz. When this signal is used in the inductive link, the resonance frequency of the inductive link is set to the carrier frequency by adding a capacitor, and narrowband signal near the resonance frequency can be transmitted effectively. However, this method is inefficient when the resonance frequency of the inductive link is unknown. Because the inductors in this work are handmade using copper wires, there is a process variation in the inductance and the f_{SR} even for the inductors with the same size. The variations of the inductor are measured as 15% for inductance value and 20% for f_{SR} , as shown in Fig. 5. These variations restrict the use of narrowband modulated signals for communication, and become the most important reason for using pulse-based inductive coupling which uses wideband signals. The difference of the received signal magnitude due to the process variation is much smaller in pulse-based inductive coupling than in narrowband inductive

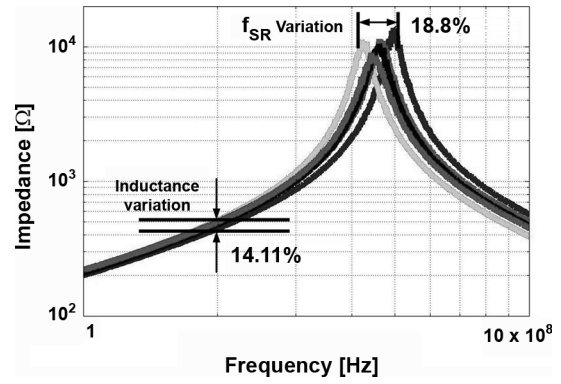


Fig. 5. Process variation for inductors with the same size (measured).

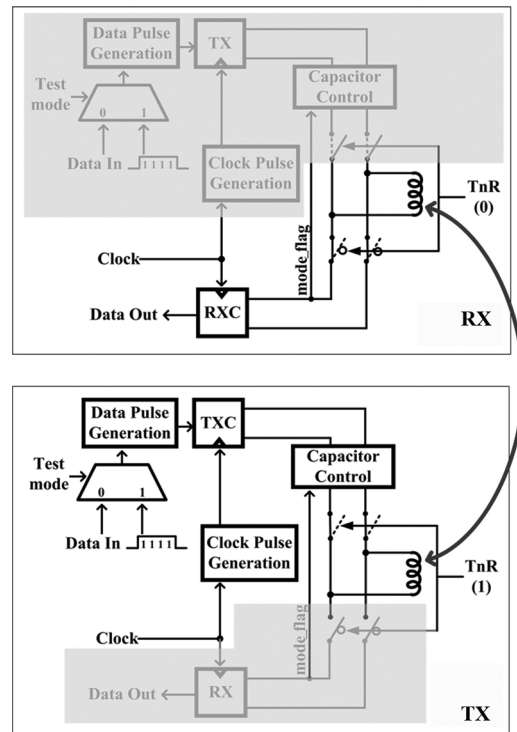


Fig. 6. Transceiver block diagram.

coupling, and this is the reason that the pulse-based inductive coupling transceiver circuits [27] can be simpler.

Although this design adopts the pulse-based inductive coupling, an on-chip parallel capacitor is used with the transmitter inductor to compensate the process variation [28]. It also plays an important role in increasing the communication range, and that will be described in detail in Section IV.

III. TRANSCEIVER OPERATION

Fig. 6 shows the block diagram of the proposed inductive coupling transceiver. The transceiver consists of a pulse generation block, a capacitor control block, and circuits for transmission and reception of data. The transmitter sends the data as a pulse, and the receiver receives the data through an inductor channel by reactive coupling and recovers the data using Schmitt triggers. The transmitter and the receiver are included in the same chip, and the transceiver can operate either as a transmitter or a receiver by setting TnR signal. In the case that the transceiver

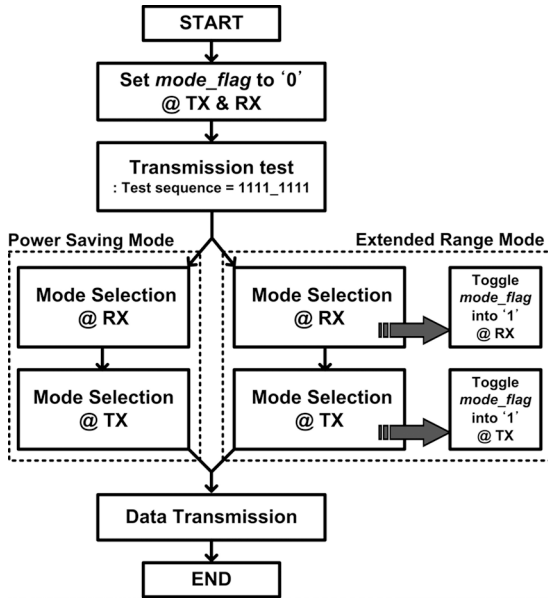


Fig. 7. Mode selection flow of the transceiver.

operates as a transmitter, the pulse generation block, capacitor control block and circuits of the transmitter are activated. On the other hand, as a receiver, only circuits of the receiver are activated as shown in Fig. 6.

There are two transmission modes in the proposed transceiver. One is power-saving mode for lower energy consumption, and the other is extended-range mode for longer communication distance. Depending on the transmission mode, the transmitter and the receiver determine whether or not the component (a capacitor or an inverter) is activated. Because both the transmitter and the receiver can operate in either transmission mode, the mode synchronization between the transmitter and the receiver is required. Fig. 7 represents the mode selection process. It is performed when the multiplexer selection signal named *Test mode* in Fig. 6 is set to 1. The *mode_flag* signal represents the mode in which the transceiver operates at that point in time; the power saving mode ($mode_flag = 0$) and the extended range mode ($mode_flag = 1$). As shown in Fig. 7, *mode_flag* signals of the transmitter and the receiver are set to 0 at the beginning of the process, so both of them operate in power saving mode. To check whether the transmission mode is proper or not, a test sequence “1111.1111” in this design is transmitted by setting the *Test mode* to 1 periodically. When the receiver receives this sequence, it sends an acknowledgment signal (ACK) to the transmitter. This ACK is related to success or failure of the test sequence transmission. To send the ACK from the receiver to the transmitter, *TnR* signals of both the transmitter and the receiver are toggled during three clock cycles after the test sequence is transmitted. At the same time, the roles of the transmitter and the receiver are changed. If the test sequence transmission is successful so that receiver can receive eight “1”s in a row, the ACK of the receiver becomes 0 and the *mode_flag* of the receiver still remains as 0. However, if the test sequence transmission fails so that the number of “1” which the receiver receives is less than eight, the ACK of the receiver becomes 1 and the *mode_flag* of the receiver toggles into 1 from 0. When the transmitter receives the ACK from the

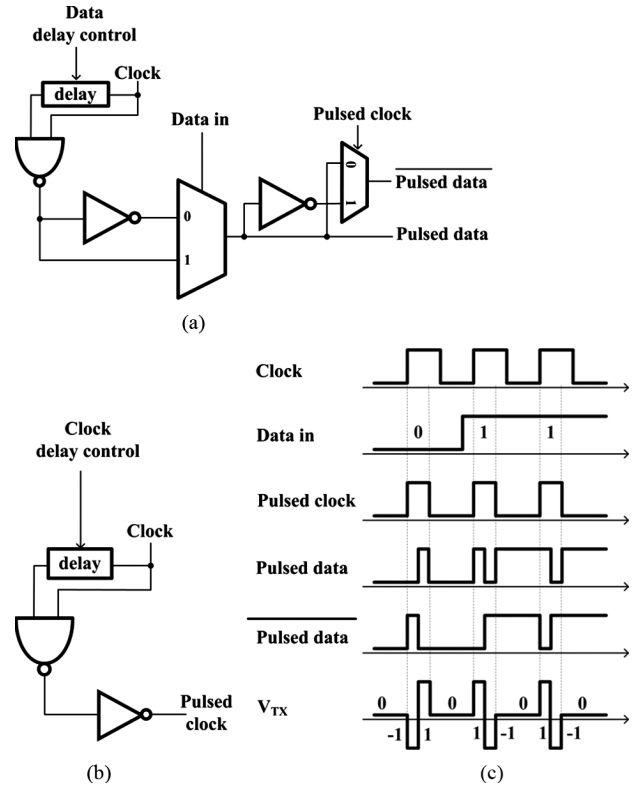


Fig. 8. Pulse-generation block. (a) Data. (b) Clock. (c) Waveforms.

receiver, it determines whether to change the *mode_flag* to 1 or not. After the mode selection process, the transmitter and the receiver operate in the same mode according to their *mode_flag*. Therefore, the percentage of the usage for each mode can be changed according to the environment. By using this adaptive mode selection technique of the transceiver, 37.5% of energy reduction can be achieved in power saving mode compared to extended range mode, and 97% of communication distance extension can be achieved in extended range mode compared to power saving mode.

IV. TRANSCIVER CIRCUITS

As shown in Fig. 6, the transceiver consists of four parts. The pulse generation block, the capacitor control block, and the transmitter circuits (TXC) serve as a part of the transmitter for reducing energy and extending communication distance, and high data rate. On the other hand, only the receiver circuits (RXC) is included the receiver.

A. Low-Energy Pulse-Generation Block

Because the inductor behaves like a short circuit for the dc voltage, the voltage pulse forced across the inductor must have a zero average value to avoid useless power dissipation. For this reason, the voltage across the transmit inductor (V_{TX}) should be shaped into the two-level pulse to reduce the unwanted direction current across the transmit inductor [29]. In this design, Manchester codes are adopted to make the two-level transmit pulse. Fig. 8 shows pulse-generation blocks of data and clock and their waveforms. The width of transmit pulses is determined by digitally controlled delay block. This pulsewidth is closely related to

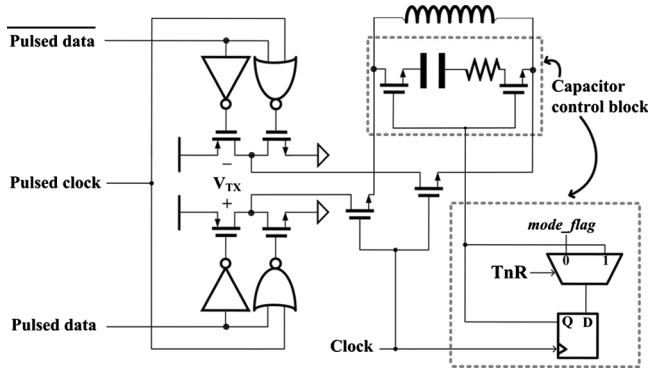


Fig. 9. Transmitter architecture.

the f_{SR} and energy consumption. In pulse-based inductive coupling, all frequency components of the pulse should be smaller than the self-resonance frequency to avoid ISI [13]. Thus, the width of the transmit pulses should be longer than the inverse of the f_{SR} . On the one hand, the energy reduction can be achieved to decrease the pulsewidth with the same slew rate [11]. Therefore, when the digital control codes of the delay block is determined, energy reduction and ISI avoidance are in tradeoff. The pulse-generation block generates the codes $(-1, 1)$ from data 0 and $(1, -1)$ from data 1, respectively.

To reduce the energy consumption, the proposed pulse-generation block employs both data pulses named *pulsed data* and *pulsed data* and clock pulses named *pulsed clock* to make two-level transmit pulses, as shown in Fig. 8. When *pulsed clock* is low, *pulsed data* and *pulsed data* are the same. And when *pulsed clock* is high, and *pulsed data* are the opposite. Therefore, as shown in Fig. 8(c), a V_{TX} is nominally zero at the low duration of *pulsed clock*, so it can reduce useless power dissipation.

B. High-Data-Rate Transmitter Circuit (TXC)

Fig. 9 represents the architecture of the transmitter. The transmitter circuit consists of H-bridge controlled by *pulsed data*, *pulsed data*, and *pulsed clock*, described in Section IV-A, and two nMOSs which are used as switches by the clock.

An H-bridge transmitter is often used in inductive coupling transceiver systems [10], [11], [22]. Most of them focus on the pulse duration control to reduce power consumption and harmonics. However, since effective ISI reduction and communication range extension are not considered seriously yet, they are additionally investigated in the proposed transmitter.

The proposed ISI reduction technique is implemented by employing two nMOSs. They act similarly as a nMOS through the

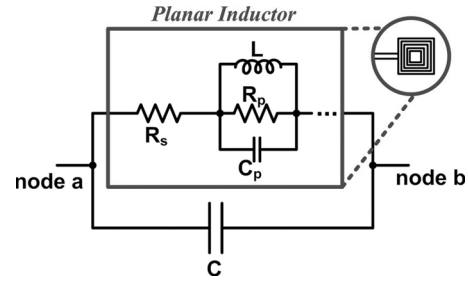


Fig. 10. RLC model of the planar inductor with on-chip parallel capacitor.

H-bridge used in [22]. Since the *pulsed clock* in the proposed pulse generation block always goes high at the rising edge of the clock, any signal in the low clock period may cause ISI. Therefore, it is needed to suppress the signals when the clock is low. In the proposed ISI reduction scheme, the transmit inductor is disconnected from the H-bridge circuits during low clock periods. Since an nMOS can block both VDD signal and GND signal well, two nMOSs are used to disconnect the transmit inductor. In this case, the nMOS transistor behaves as a resistor to transmit signals. Also, by increasing the width of these nMOSs, we can minimize the degradation of transmit signals. By using this method, the data rate can be increased by 14% compared to the conventional method.

C. Capacitor Control Block

Capacitor control block serves as the dual mode operation of the transmitter. When the transmitter operates in extended range mode, capacitor control block connects the on-chip parallel capacitor with the transmit inductor. On the other hand, in power saving mode, capacitor control block does not connect the capacitor. An enhancement of communication distance can be achieved in extended range mode since the impedance between both ends of the inductor is increased when the capacitor is connected in parallel with the inductor at all frequencies which includes the data signal components. Fig. 10 shows the RLC model of the planar inductor with the additional parallel capacitor. The RLC model of the planar inductor is same as in Fig. 2. And the additional on-chip capacitor C is connected to the planar inductor. The impedance between node a and node b is derived as shown in (7) at the bottom of the page. By comparing (4) and (7), the only difference between with and without a parallel capacitor is the term

$$-\omega^2 LC(R_S + R_P) + j\omega CR_S R_P(1 - \omega^2 LC_P). \quad (8)$$

$$\begin{aligned} Z_{ab} &= \left\{ \left(j\omega L \parallel R_P \parallel \frac{1}{j\omega C_P} \right) + R_S \right\} \parallel \frac{1}{j\omega C} \\ &= \frac{j\omega L(R_S + R_P) + R_S R_P(1 - \omega^2 LC_P)}{R_P(1 - \omega^2 LC_P) - \omega^2 LC(R_S + R_P) + j\{\omega L + \omega CR_S R_P(1 - \omega^2 LC_P)\}} \end{aligned} \quad (7)$$

in the denominator of (7). Assuming the impedance of the planar inductor itself is Z_1 , and the impedance of the planar inductor with a parallel capacitor C is Z_2 . Then, the impedances are

$$\begin{aligned} Z_1 &= \alpha + j\beta \\ Z_2 &= (\alpha - \chi) + j(\beta + \delta) \end{aligned} \quad (9)$$

where

$$\begin{aligned} \alpha &= R_P(1 - \omega^2 LC_P) \\ \beta &= \omega L \\ \chi &= \omega^2 LC(R_S + R_P) \\ \delta &= \omega CR_S R_P(1 - \omega^2 LC_P). \end{aligned}$$

To achieve the merits of connecting a parallel capacitor C , the difference between squares of Z_1 and Z_2 must be larger than zero as

$$\begin{aligned} (\sqrt{\alpha^2 + \beta^2})^2 - (\sqrt{(\alpha - \chi)^2 + (\beta + \delta)^2})^2 \\ = 2\alpha\chi - \chi^2 - 2\beta\delta - \delta^2 > 0. \end{aligned} \quad (10)$$

From the above condition, the following condition is derived:

$$2\alpha\chi - \chi^2 - 2\beta\delta - \delta^2 > 0, \quad \chi > \frac{\chi^2 + 2\beta\delta + \delta^2}{2\alpha}. \quad (11)$$

For the pulse-based inductive coupling transceiver, all frequencies that are included in the signal components must be smaller than f_{SR} of the planar inductor to avoid ISI. According to [30], bandwidth of at least twofold of signal bandwidth is required for inductive coupling to dampen the received signal and to diminish ISI. Therefore, based on S - and Z -parameter analysis of the planar inductor, we can determine the upper limit of the frequency for inductive coupling communication to the half of f_{SR} of the planar inductor as

$$\omega \leq \frac{1}{2\omega_{sf}} = \frac{1}{2\sqrt{LC_P}}. \quad (12)$$

By using $\omega = 1/2\sqrt{LC_P}$, which is the upper bound frequency of the signal, the expressions for σ , β , χ , and δ in (9) can be simplified as

$$\begin{aligned} \alpha &= \frac{3}{4}R_P \quad \chi = \frac{C}{4C_P}(R_S + R_P) \\ \beta &= \frac{1}{2}\sqrt{\frac{L}{C_P}} \quad \delta = \frac{3}{8\sqrt{LC_P}}CR_S R_P. \end{aligned} \quad (13)$$

Also, considering the values in Table I, the magnitude conditions in (13) are as follows:

$$\begin{aligned} \chi &\gg \delta \\ \chi^2 &\gg 2\beta\delta. \end{aligned} \quad (14)$$

Therefore, the on-chip parallel capacitor should keep to the condition

$$\begin{aligned} \frac{C}{4C_P}(R_S + R_P) &< \frac{3}{2}R_P \\ \therefore C &< 6C_P. \end{aligned} \quad (15)$$

TABLE I
PARAMETERS OF THE INDUCTOR

Symbol	Description	Value
L	Inductance	2 μ H
f_{SR}	Self-resonance frequency	400MHz
C_P	Parasitic capacitance	79fF
R_P	Parasitic resistance	13k Ω
R_S	Resistance	3 Ω
α	Capacitance ratio (C/C_P)	0.5
C	On-chip capacitance	40fF

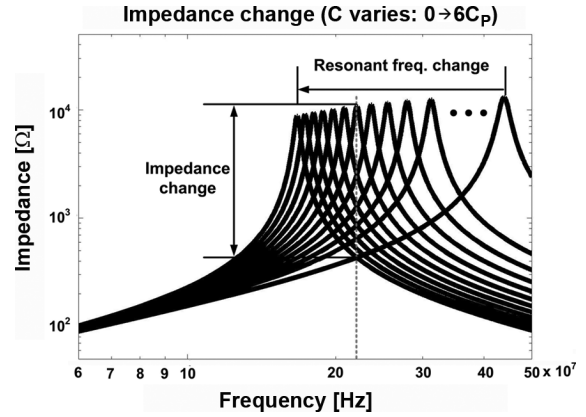


Fig. 11. Z -parameter variation of node a—node b (Fig. 10) when the capacitance changes from 0 to $6C_P$ (simulation).

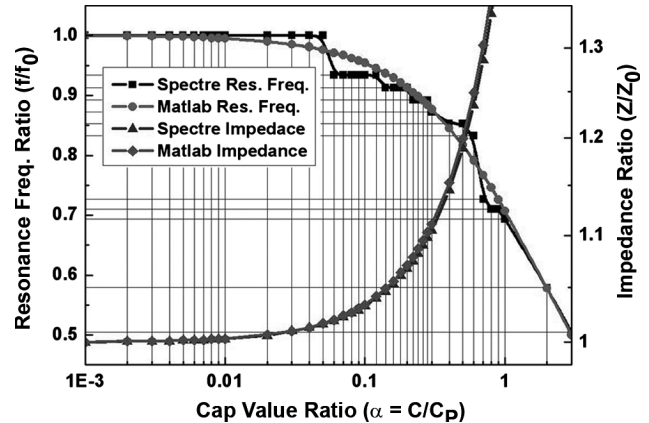


Fig. 12. Z and self-resonance frequency versus capacitance at $\omega = 1/2\sqrt{LC_P}$ (simulation).

The other condition for the capacitance is about the resonance frequency of the inductive link. When the additional capacitance is large enough compared with the parasitic capacitance of the inductor C_P , the resonance frequency is dominated by this additional capacitance, and can be significantly decreased compared to the f_{SR} if the additional capacitance is too large.

Fig. 11 shows how the impedance between node a and node b (Fig. 10) changes according as the capacitance C , varying from 0 to $6C_P$. As the capacitance gets larger, resonance frequency of the planar inductor with the parallel capacitor becomes lower. Also the impedance is increased at all frequencies which are lower than the half of f_{SR} . On the other hand, depending on the parallel capacitor value, the impedance at frequency $> 1/2f_{SR}$

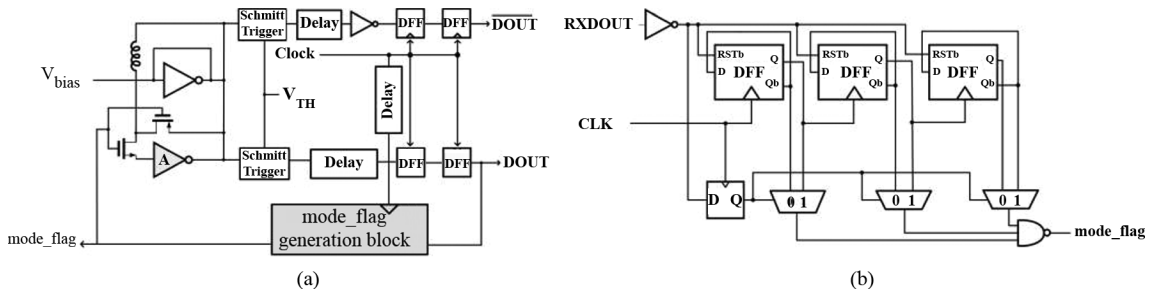


Fig. 13. (a) Receiver architecture. (b) Mode flag generation block.

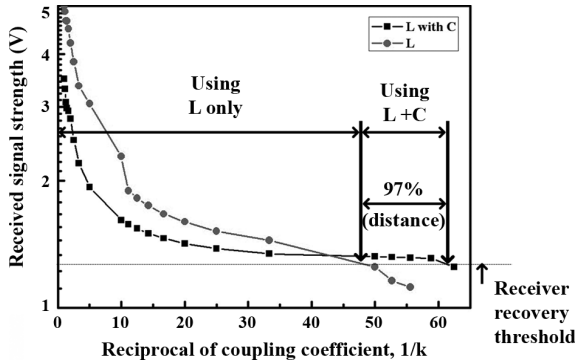


Fig. 14. Received signal strength versus reciprocal of coupling coefficient 1/k (measurement).

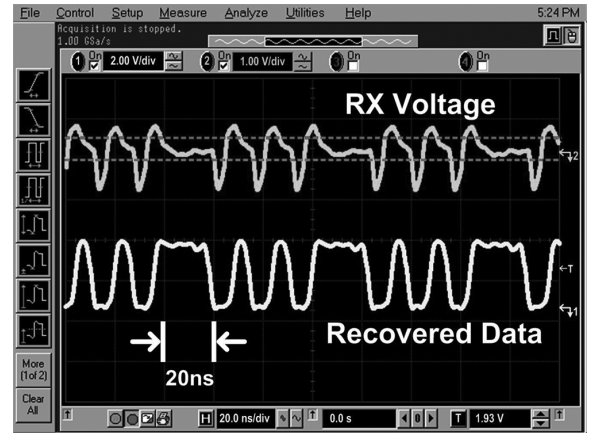


Fig. 16. Board measurement result using discrete components.

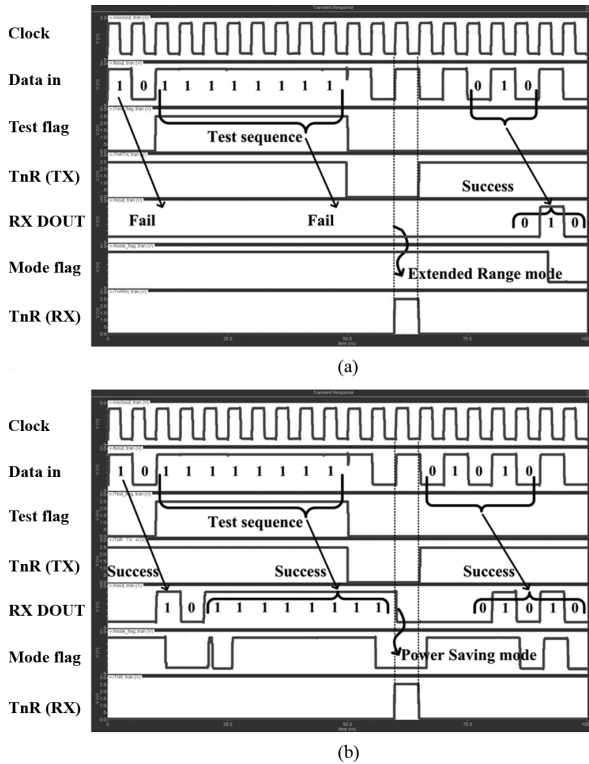


Fig. 15. Data transfer simulation waveform at 200 Mbps (a) $k = 0.02$ (b) $k = 0.7$.

is increased or decreased. Since the impedance of the transmitter inductor becomes larger, the received signal strength becomes larger. It represents the signal can be transmitted success-

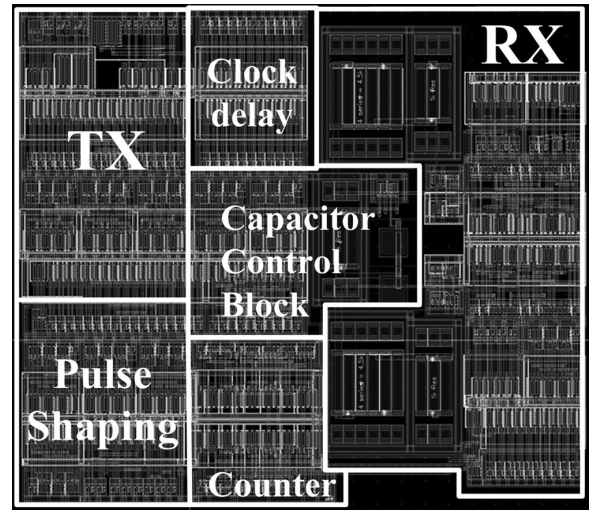


Fig. 17. Layout photo (0.12 mm × 0.1 mm except pads).

fully at longer distance. Fig. 12 shows the relationship between the impedance, f_{SR} , and the capacitance. Simulations are performed with Matlab and Spectre. Both simulation results show the increase in impedance and decrease in resonance frequency as capacitance becomes larger. Considering three factors of the communication distance increase, potential data rate decrease, and power consumption increase, capacitance ratio α is set to 0.5. At this value, the impedance is increased by 20%, and the resonance frequency is decreased by 15%. Because we use the signal frequency only up to the half of f_{SR} , 15% decrease of resonance frequency does not affect the data rate.

TABLE II
PERFORMANCE COMPARISON

REF. No.	ISSCC [7]	TCAS [9]	JSSC [11]		ESSCIRC [22]	This work		
						Power saving	Extended range	
CMOS process	0.18 μ m	90nm	90nm	0.18 μ m	90nm	0.25μm		
Data rate	400Mbps	5Gbps	1Gbps		50Mbps	200Mbps		
Power consumption	TX	99mW	3mW	110mW	130mW	565 μ W	2.2mW	2.3mW
	RX	137mW	6mW	30mW	200mW	3.6mW	1.8mW	4.1mW
Energy consumption	TX	250pJ/b	0.6fJ/b	0.11pJ/b	0.13pJ/b	11.3pJ/b	11pJ/b	11pJ/b
	RX	340pJ/b	1.2fJ/b	0.03pJ/b	0.2pJ/b	72pJ/b	9pJ/b	21pJ/b
Wireless Interface	UWB	IR-UWB	Inductive coupling		Inductive coupling (76nH for TRX)	Inductive coupling (2μH for TRX)		
Communication distance	-	0.03mm	0.015mm		50mm	30mm	59mm	
Type of Result	Measurement	Simulation	Measurement		Measurement	Simulation		

D. Receiver Circuit (RXC)

Fig. 13(a) shows the architecture of the receiver. It consists of two Schmitt triggers, four-D-flip-flops, several inverters, and a mode flag generation block. To make the transmitter and the receiver operates in the same mode, *mode_flag* is sent to the transmitter from the receiver in order to control the capacitor control block in the transmitter. The inverter A serves as the dual mode operation of the receiver. When the receiver operates in power saving mode, *mode_flag* is zero and two nMOS switches are turned off. In this case, the inverter A is disconnected from the receiver circuits. On the other hand, in extended range mode, two nMOS switches are switched on and the inverter A is connected to other circuits. Using the inverter A causes power consumption to be increased, but makes the receiver sensitivity increase. Therefore, it can be used for detecting much smaller signals in extended range mode.

The mode flag generation block diagram is shown in Fig. 13(b). It consists of a three-input NAND gate, three multiplexers, a 3-b counter, and a D-flip-flop. *Mode_flag* is used to change the transmission mode in the receiver, and sent to the transmitter to make the same operation mode in the transmitter and the receiver. The only case that *mode_flag* becomes 0 is that the input sequence “1111_1111” is detected correctly; otherwise, a 3-b counter is reset to zero. When *Test mode* in the transmitter is set to 1, the *mode_flag* of the receiver can be sent to the transmitter, since *TnR* signal is toggled at that point. If *mode_flag* received at the transmitter is 0, the transmitter operates in power saving mode; otherwise, it operates in extended range mode as described in Section III.

Fig. 14 presents the relationship between the received signal strength and the reciprocal of the coupling coefficient $k(1/k)$ at 200 Mbps ($1/k$ is proportional to the communication distance as shown in Fig. 4). Therefore, Fig. 14 also means the relationship between the received signal strength and the communication distance. The distance between the transmitter and the receiver can be modeled as a function of k based on the measurements. Fig. 14 shows that the upper bound of the transmission distance in power saving mode is 30 mm, with $k = 0.0212$. In contrast, extended range mode allows the communication distance up to 59 mm at which $k = 0.017$. Therefore, the inductor

is used alone for the communication distance within 30 mm, and the parallel capacitor is used together with the inductor for the communication distance over 30 mm. By adaptively choosing the use of a parallel capacitor, the transceiver can reduce the power consumption and extend the communication distance in each transmission mode.

V. PERFORMANCE EVALUATION

Fig. 15 shows the simulation results of the data transmissions at 200 Mbps. The coupling coefficient k of the simulation is 0.02 and 0.7, respectively. In the case $k = 0.02$, as shown in Fig. 15(a), the transceiver operates in power saving mode, but the data transmission fails. When *Test flag* is set to 1, the transmitter sends the test sequence of “1111_1111” to the receiver and the receiver cannot recover it correctly. So the transmission mode of the receiver is changed to extended range mode. During that operation, *TnR* signal of the transmitter is toggled to 0 so that the transmitter can receive the ACK from the receiver. After the transmission modes of the transmitter and the receiver switches to the extended range mode, the data transmission becomes successful. On the other hand, when $k = 0.7$, the transceiver operates in power saving mode successfully, as shown in Fig. 15(b). Therefore, after the mode selection process, the transmission mode does not change and the transmission is still successful. To verify the possibility of the proposed transceiver, measurements using discrete components were performed as shown in Fig. 16. The data rate is limited by on-board transmitter, up to 125 Mbps. If the chip is implemented, the data rate can be increased up to 200 Mbps as the simulation. Fig. 17 shows the layout using 0.25- μ m standard CMOS technology. The layout area excluding pads is 0.012 mm².

The performance comparison with other works is shown in Table II with respect to data rate, energy consumption, and the communication distance. The proposed transceiver of this work shows low energy consumption and comparable or longer communication distance with high data rate among other research.

VI. CONCLUSION

A 200-Mbps 0.02-nJ/b dual-mode inductive coupling transceiver is designed and simulated in 0.25- μ m CMOS process.

The important issues of this design are data-rate increase, communication distance enhancement, and low energy consumption. To achieve them, the pulse generation scheme, the parallel capacitor with the transmit inductor, and the ISI reduction scheme are newly proposed. The pulse generation scheme makes the transceiver consume 0.02 nJ/b energy under 2.5-V supply voltage. An effective ISI reduction scheme enhances the data rate up to 200 Mbps. By employing an adaptively enabled parallel capacitor, the dual mode operation of the transceiver can be performed in order to trade off between the low-energy consumption and the communication distance enhancement. The transceiver takes 0.012 mm² area at 0.25- μ m CMOS process.

REFERENCES

- [1] J. Karaoqoz, "High-rate wireless personal area networks," *IEEE Commun. Mag.*, vol. 39, no. 12, pp. 96–102, Dec. 2001.
- [2] B. Allen, T. Brown, K. Schwieger, E. Zimmermann, W. Malik, D. Edwards, L. Ouvry, and I. Oppermann, "Ultra wideband: Applications, technology and future perspectives," in *Proc. Int. Workshop on Convergent Technologies*, 2005, pp. 1–6.
- [3] K. Eom and H. Arai, "A free access mat by tightly coupled patch array for short range wireless access," in *Proc. IEEE Antennas and Propag. Int. Symp.*, Jun. 2007, pp. 441–444.
- [4] K. Eom and H. Arai, "Dual band free access mat for short range wireless access," in *Proc. 18th Annu. IEEE Int. Symp. Personal, Indoor and Mobile Radio Communications (PIMRC)*, 2007, pp. 1–5.
- [5] J.-S. Lee, Y.-W. Su, and C.-C. Shen, "A comparative study of wireless protocols: Bluetooth, UWB, ZigBee, and Wi-Fi," in *Proc. 33rd Annu. Conf. IEEE Ind. Electron. Soc. (IECON)*, Taipei, Taiwan, Nov. 5–8, 2007, pp. 46–51.
- [6] P.-I. Mak and R. P. Martins, "Transceiver architecture selection: Review, state-of-the art survey and case study," *IEEE Circuits Syst. Mag.*, vol. 7, no. 2, pp. 6–25, Feb. 2007.
- [7] Y. Zheng, K.-W. Wong, M. A. Asaru, D. Shen, W. H. Zhao, Y. J. The, P. Andrew, F. Lin, W. G. Yeoh, and R. Singh, "A 0.18 μ m CMOS dual-band UWB transceiver," in *Proc. IEEE Int. Solid-State Circuits Conf.*, Feb. 2007, pp. 114–590.
- [8] J. Ryckaert, C. Desset, A. Fort, M. Badaroglu, V. D. Heyn, P. Wambacq, G. V. Plas, S. Donnay, B. V. Poucke, and B. Gyselinckx, "Ultra-wide-band transmitter for low-power wireless body area networks: Design and evaluation," *IEEE Trans. Circuits Syst. I, Reg. Papers*, vol. 52, no. 12, pp. 2515–2525, Dec. 2005.
- [9] Y. Wang, A. M. Niknejad, V. Gaudet, and K. Iniewski, "A CMOS IR-UWB transceiver design for contact-less chip testing applications," *IEEE Trans. Circuits Syst. II, Exp. Briefs*, vol. 55, no. 4, pp. 334–338, Apr. 2008.
- [10] N. Miura, D. Mizoguchi, M. Inoue, K. Niitsu, Y. Nakagawa, M. Tago, M. Fukaishi, T. Sakurai, and T. Kuroda, "A 1 Tb/s 3W inductive-coupling transceiver for 3D-Stacked inter-chip clock and data link," *IEEE J. Solid-State Circuits*, vol. 42, no. 1, pp. 111–122, Jan. 2007.
- [11] N. Miura, H. Ishikuro, K. Niitsu, T. Sakurai, and T. Kuroda, "A 0.14 pJ/b inductive-coupling transceiver with digitally-controlled precise pulse shaping," *IEEE J. Solid-State Circuits*, vol. 43, no. 1, pp. 285–291, Jan. 2008.
- [12] H. Ishikuro, T. Sugahara, and T. Kuroda, "An attachable wireless chip access interface for arbitrary data rate using pulse-based inductive-coupling through LSI package," in *Proc. IEEE Int. Solid-State Circuits Conf.*, 2007, pp. 360–608.
- [13] H. Ishikuro, N. Miura, and T. Kuroda, "Wideband inductive-coupling interface for high-performance portable system," in *Proc. IEEE Custom Integrated Circuits Conf. (CICC)*, 2007, pp. 13–20.
- [14] R. Bashirullah, W. Liu, Y. Ji, A. Kendir, M. Sivaprakasam, G. Wang, and B. Pundi, "A smart bi-directional telemetry unit for retinal prosthetic device," in *Proc. IEEE Int. Symp. Circuits Syst.*, 2003, pp. V-5–V-8.
- [15] M. S. Wegmueller, M. Hediger, T. Kaufmann, F. Buerger, and W. Fichtner, "Wireless implant communications for biomedical monitoring sensor network," in *Proc. IEEE Int. Symp. Circuits Syst.*, 2007, pp. 809–812.
- [16] Z. Lu and M. Sawan, "An 8 Mbps data rate transmission by inductive link dedicated to implantable devices," in *Proc. IEEE Int. Symp. Circuits Syst.*, 2008, pp. 3057–3060.
- [17] Y. Hu and M. Sawan, "A fully integrated low-power BPSK demodulator for implantable medical devices," *IEEE Tran. Circuits Syst. I, Reg. Papers*, vol. 52, no. 12, pp. 2552–2562, Dec. 2005.
- [18] C. Sauer, M. Stanačević, G. Cauwenberghs, and N. Thakor, "Power harvesting and telemetry in CMOS for implanted devices," *IEEE Trans. Circuits Syst. I, Reg. Papers*, vol. 52, no. 12, pp. 2605–2613, Dec. 2005.
- [19] M. Ghovanloo and S. Atluri, "A wideband power-efficient inductive wireless link for implantable microelectronic devices using multiple carriers," *IEEE Trans. Circuits Syst. I, Reg. Papers*, vol. 54, no. 10, pp. 2211–2221, Oct. 2007.
- [20] P. Li and R. Bashirullah, "A wireless power interface for rechargeable battery operated medical implants," *IEEE Trans. Circuits Syst. II, Exp. Briefs*, vol. 54, no. 10, pp. 912–916, Oct. 2007.
- [21] M. Nowak, E. Colinet, F. Conseil, and G. Jacquemod, "A wireless sensing platform for battery-free sensors," in *Proc. IEEE Int. Symp. Circuits Syst.*, 2008, pp. 2122–2125.
- [22] D. Guermandi, S. Gambini, and J. Rabaey, "A 1 V 250 kpps 90 nm CMOS pulse based transceiver for cm-range wireless communication," in *Proc. IEEE Eur. Solid-State Circuits Conf.*, Sep. 2007, pp. 135–138.
- [23] I. Locher, H. Junjer, T. Kirstein, and G. Tröster, "Wireless, low-cost interface for body area networks," in *Proc. IEEE Int. Symp. Wearable Computers (ISWC)*, 2004, pp. 170–171.
- [24] H. A. Wheeler, "Simple inductance formulas for radio coils," *Proc. IRE*, vol. 16, no. 10, Oct. 1928.
- [25] D. C. Daly and A. P. Chandrakasan, "An energy-efficient OOK transceiver for wireless sensor networks," *IEEE J. Solid-State Circuits*, vol. 42, 5, May 2007.
- [26] J. Ryu, M. Kim, J. Lee, B.-S. Kim, M.-Q. Lee, and S. Nam, "Low power OOK transmitter for wireless capsule endoscope," in *IEEE/MTT-S Int. Microw. Symp.*, 2007, pp. 855–858.
- [27] D. C. Yates, A. S. Holmes, and A. J. Burdett, "Optimal transmission frequency for ultralow-power short-range radio links," *IEEE Trans. Circuits Syst. I, Reg. Papers*, vol. 51, no. 7, pp. 1405–1413, Jul. 2004.
- [28] J. Yoo, S. Lee, and H.-J. Yoo, "A 1.12 pJ/b resonance compensated inductive transceiver with a fault-tolerant network controller for wearable body sensor networks," in *Proc. IEEE Asian Solid-State Circuits Conf. (A-SSCC)*, 2008, pp. 313–316.
- [29] D. Guermandi, S. Gambini, and J. Rabaey, "Short Range Pulse Based Inductive Transceiver," Dept. of Electron. Eng. and Comput. Sci., Univ. of California, Berkeley, 2006, Tech. Rep. UCB/EECS-2006-155.
- [30] N. Miura, D. Mizoguchi, M. Inoue, T. Sakurai, and T. Kuroda, "A 195-Gb/s 1.2-W inductive inter-chip wireless superconnect with transmit power control scheme for 3-D-Stacked system in a package," *IEEE J. Solid-State Circuits*, vol. 41, 1, Jan. 2006.
- [31] S. Lee, J. Yoo, and H.-J. Yoo, "A 200 Mbps 0.02 nJ/b dual-mode inductive coupling transceiver for cm-range interconnection," in *Proc. IEEE Int. Symp. Circuits Syst.*, 2008, pp. 1954–1957.



Sulki Lee (S'07) received the B.S. and M.S. degrees from Korea Advanced Institute of Science and Technology (KAIST), Daejeon, in 2007 and 2009, respectively, where she is currently working toward the Ph.D. degree, all in electronic engineering.

Her current research interests include the inductive coupling transceiver design and near-field communication.



Jerald Yoo (S'05) received the B.S. and M.S. degrees from the Korea Advanced Institute of Science and Technology (KAIST), Daejeon, Korea, in 2002 and 2007, respectively, where he is currently working toward the Ph.D. degree, all in electrical engineering.

He has worked on developing the embedded processor for PRAM and the digital signal processor for a digital hearing aid. His current research interests include communication transceivers for energy-efficient body area network, fabric area network, and wireless power transmission and low-power biomedical microsystems.



Hoi-Jun Yoo (M'95–SM'04–F'08) received the B.S. degree from Seoul National University, Seoul, Korea, in 1983 and the M.S. and Ph.D. degrees in electrical engineering from the Korea Advanced Institute of Science and Technology (KAIST), Daejeon, in 1985 and 1988, respectively. His Ph.D. work concerned the fabrication process for GaAs vertical optoelectronic integrated circuits.

From 1988 to 1990, he was with Bell Communications Research, Red Bank, NJ, where he invented the 2-D phased-locked VCSEL array, the front-surface-emitting laser, and the high-speed lateral HBT. In 1991, he became Manager of a DRAM design group at Hyundai Electronics and designed a family of fast-1M DRAMs and 256 M synchronous DRAMs. In 1998, he joined the faculty of the Department of Electrical Engineering at KAIST and now is a full Professor. From 2001 to 2005, he was the Director of System Integration and IP Authoring Research Center (SIPAC), funded by the Korean government to promote worldwide IP authoring and its SoC application. From 2003 to 2005,

he was the full-time Advisor to the Minister of Korea Ministry of Information and Communication and National Project Manager for SoC and Computer. In 2007, he founded SDIA (System Design Innovation and Application Research Center) at KAIST to research and develop SoCs for intelligent robots, wearable computers and biosystems. His current interests are high-speed and low-power network on Chips, 3-D graphics, body area networks, biomedical devices and circuits, and memory circuits and systems. He is the author of the books *DRAM Design* (Hongleung, 1996, in Korean), *High Performance DRAM* (Sigma, 1999, in Korean), and chapters of *Networks on Chips* (Morgan Kaufmann, 2006).

Dr. Yoo was the recipient of the Electronic Industrial Association of Korea Award for his contribution to DRAM technology the 1994, Hynix Development Award in 1995, the Korea Semiconductor Industry Association Award in 2002, the Best Research of KAIST Award in 2007, the Design Award of 2001 ASP-DAC, and Outstanding Design Awards 2005, 2006, 2007 A-SSCC. He is a member of the executive committee of ISSCC, Symposium on VLSI, and A-SSCC. He was the TPC chair of A-SSCC 2008.